The influence of electron reflection at the electrode and secondary electron emission on a strongly magnetized low-pressure RF discharge

1996 J. Phys. D: Appl. Phys. 29 378

(http://iopscience.iop.org/0022-3727/29/2/014)

J. Phys. D: Appl. Phys. **29** (1996) 378–387. Printed in the UK

The influence of electron reflection at the electrode and secondary electron emission on a strongly magnetized low-pressure RF discharge

Ralf Krimke and Herbert M Urbassek

Fachbereich Physik, Universität Kaiserslautern, Erwin-Schrödinger-Straße, D-67663 Kaiserslautern, Germany

Received 10 July 1995

Abstract. With the help of a particle-in-cell/Monte Carlo simulation, we study a strongly asymmetric cylindrical low-pressure RF discharge in an axial magnetic field. In particular, the effects of electron reflection from the electrodes and of ion-induced secondary electron emission are studied. The process alone does not change the plasma characteristics; this fact can be traced back to the gyro-motion of electrons in the electrode sheath, which brings non-colliding electrons back to the electrode. If electron reflection is allowed for, the overall plasma density is substantially increased. This effect is found qualitatively in experiments. We furthermore demonstrate the existence of high-energy electrons throughout the bulk plasma; this fact is reminiscent of the well-known γ-regime of unmagnetized RF discharges.

1. Introduction

It has been known for some 50 years that secondary electrons are vital for operating a self-sustaining DC discharge. RF discharges, on the other hand, can be operated continuously without secondary electrons. Here, secondary electrons, if present, may strongly change the characteristics of a discharge; it changes from the so-called α- to the γ-regime [1–5]. The characteristics of both regimes, and of their transition, have been intensely studied in the past [6–10].

The case of a discharge in an external magnetic field applied parallel to the electrodes is more complex. Here, recent investigations give conflicting results in predicting no, or no considerable influence [11–14]; on the other hand, there are experiments which show that a careful choice of the electrode material can substantially increase the plasma density [15, 16]; the origin of this influence is traced back to the secondary electron emission coefficient of the material.

In the present study we wish to shed light on the question of how the secondary electron emission from the electrodes can influence the discharge characteristics in a magnetized plasma. To this end, we perform a kinetic simulation of a low-pressure cylindrical discharge in an axial magnetic field; this discharge has been studied in some detail in the past for inert electrodes [17]. These latter studies can be used as a reference case against which we can compare the present investigations.

2. The system

The model discharge is confined by two co-axial electrodes of radii $r_0 = 0.5$ cm, $r_1 = 3.5$ cm and height $h = 4.5$ cm. A schematic sketch is shown in figure 1. Whereas the outer electrode is earthed, the inner electrode is coupled by a capacitance C to a voltage source

$$V(t) = V_{RF} \sin(\omega_{RF} t). \tag{1}$$

Thus, if φ denotes the phase in the RF cycle then $V(\varphi = \pi/2)$ is the maximum positive potential at the inner electrode. An external, homogeneous magnetic field of strength $B = 7$ mT is applied in the axial direction. For the electrons of mass m_e and charge $-e$ the gyration frequency is $\omega_{c,e} = eB/m_e = 1.2 \times 10^9$ s^{-1}. The external capacitance is chosen to be $C = 10$ pF. The RF voltage amplitude and circular frequency were set to $V_{RF} = 500$ V and $\omega_{RF} = 2\pi \times 13.56$ MHz.

The discharge vessel is filled with argon at temperature $T_0 = 300$ K and pressure $p_0 = 1.36$ mTorr. Electrons and Ar^+ ions are the only charged species assumed to be relevant in the discharge. They interact with the neutral argon atoms by the following processes: electrons may scatter elastically [18], they may ionize [19] or they may excite the atoms from the ground state. The excitation cross section is summed over all 4s, 4p, 3d and 5s final states [20]. Ions may scatter elastically or by charge exchange

0022-3727/96/020378+10$19.50

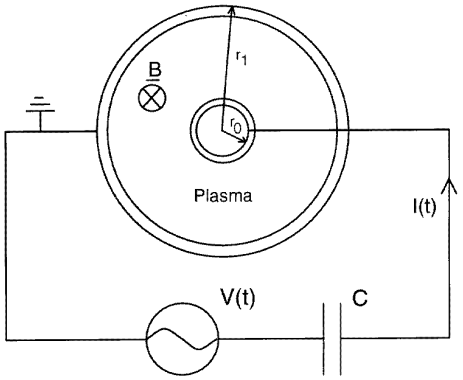

Figure 1. A schematic diagram of the model discharge.

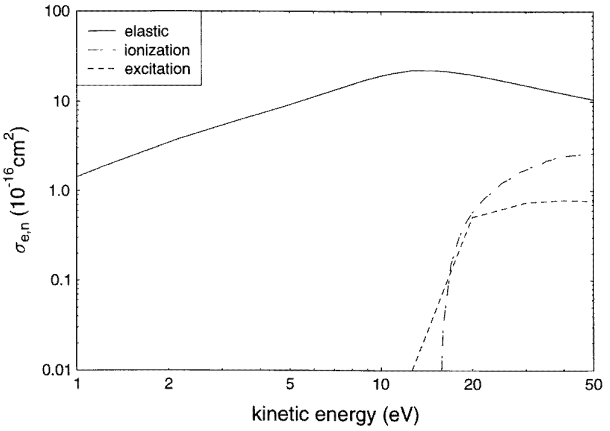

Figure 2. Electron–neutral argon collision cross sections, as used in the simulation.

from atoms. The total scattering cross sections of the electrons are given in figure 2; for the ions we use data given by [21].

2.1. Secondary electrons

The presence of electrodes in contact with the discharge plasma makes it necessary to consider particle–surface interactions (PSI). The nature of these interactions is complex and an active field of research in its own right. A full incorporation of these interactions is beyond the possibility of today's computer resources and modelling techniques. Most important of all PSI phenomena is the electron emission from the surface; it exerts a strong influence on the temperature and density of the plasma [22]. We therefore restrict our analysis of PSI to electron emission. Thereby the characteristics of the electrodes in our model discharge are not necessarily chosen in such a way as to resemble those of a specific real solid. We rather employ a configuration which illustrates the possible influence of PSI on our discharge.

A detailed description of various electron emission processes has been given in [23, 24]. Thermal electron emission can be neglected for our cold electrodes. The low density of photons in the discharge and the small yields of less than 0.1 electron per photon render photon-induced electron emission irrelevant to glow discharges.

Two important processes are included in our simulation model, (i) electron reflection and (ii) ion-induced secondary electron emission:

(i) A description of secondary electron emission induced by electron beams on solids has been given in [25]. There it is shown that the backscattering coefficient η for electrons can be considerable at incident electron energies around 100 eV. The backscattering mechanism is reviewed in [26] in more detail. For oblique incidence η increases and the backscattered electrons are reflected in the specular direction. We consider elastic specular reflection of the electrons at the surface with a probability in the range of $\eta = 0$–0.8. Inelastic electron scattering and secondary electron emission due to electron bombardment are neglected.

(ii) Experimental results are available for ion-induced electron emission; the electron emission coefficient γ_i for argon ions, particularly on metal surfaces was investigated in [27]. The general principles and mechanisms of ion-induced electron emission have been described in [28]. Because of the relatively low kinetic energy of the ions hitting the electrodes ($E_{kin,i} < 1000$ eV), only the potential emission is of importance in this discharge. In [29] an empirical relation for potential emission due to low-energy ion bombardment on metal surfaces is given:

$$\gamma_i = 3.2 \times 10^{-3}(0.78\mathcal{E}_{ion} - 2\mathcal{W}) \qquad (2)$$

where $\mathcal{E}_{ion}$ is the ionization energy of the incident ion and $\mathcal{W}$ is the work function of the metal target. In our model we consider ion-induced secondary electron emission at the inner electrode with an emission coefficient γ_i calculated according to equation (2) with the ionization energy of argon $\mathcal{E}_{ion} = 15.76$ eV and a workfunction $\mathcal{W}$, which is in the range of 0.5–4 eV.

The kinetic energy of neutral atoms bombarding the electrode is at most that of ions which undergo an ion-neutral charge exchange collision in the sheath. This energy is not sufficiently high to induce kinetic electron emission from the surface. Potential emission does not take place for neutral atoms. Therefore secondary electron emission due to neutral atom impact is of no importance in this type of discharge.

2.2. The kinetic simulation model

The non-local structure of the sheaths and a microscopic description of the secondary electron processes require a kinetic code for a self-consistent simulation. We use the particle-in-cell Monte Carlo method (PIC/MC) [30]. Our simulation scheme is based on the one-dimensional PDC1 code [31] and was described previously [17]. The gas discharge is simulated using 24 000–48 000 pseudo-electrons and pseudo-ions. Each of the pseudo-particles represents 4×10^7 real particles. The particles are represented via their radial position r and their velocity components v_r, v_ϑ and v_z in the radial, azimuthal and axial

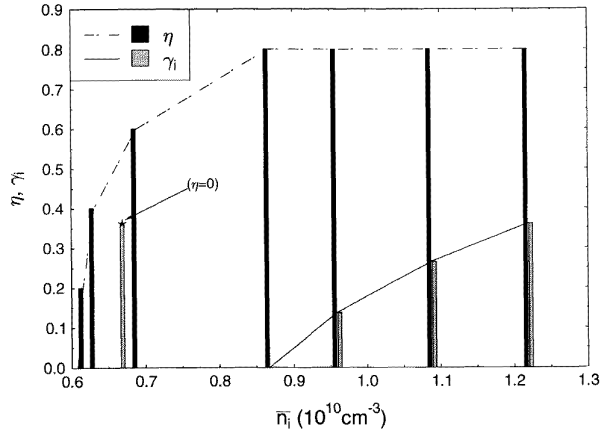

Figure 3. The coefficients of electron reflection η and ion-induced secondary electron emission γ_i plotted versus the average ion density $\overline{n_i}$ in the discharge. Note the special case of $(\eta, \gamma_i) = (0, 0.36)$, denoted by an asterisk.

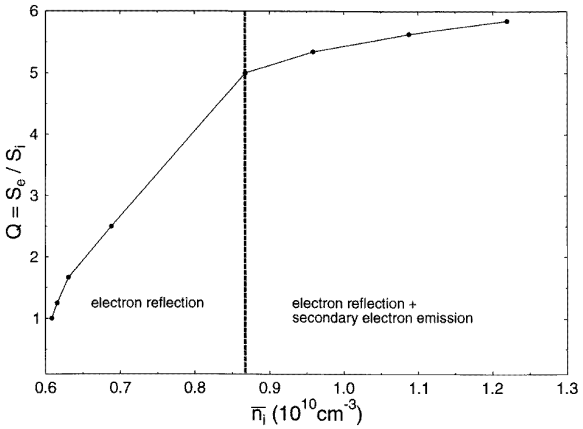

Figure 4. The quotient Q of electron production rate S_e and ion production rate S_i for different discharges.

directions. A linear weighting scheme is used to calculate the charge density on an underlying linear radial grid. The electric field generated by all particles is calculated via Poisson's equation on the grid. The boundary conditions of the discharge are determined consistently with the solution of the external circuit equations. The particles move under their self-consistent electric field and the external magnetic field. Their collisions with neutral species are simulated using an MC algorithm based on predetermined cross sections.

The cell width and the time step were chosen as $\Delta r = 0.006$ cm and $\Delta t = 36$ ps. To improve the statistics we used a particle splitting scheme in the sheaths. A subcycling algorithm was implemented in the bulk of the plasma to lower the computational cost of the simulation [32, 33]. The code was adapted to its use on a multiple instructions multiple data (MIMD) machine. In this way the computer resources of parallel computers and workstation clusters could be made available. Part of the simulations were performed on an Intel PARAGON parallel computer with 134 nodes.

We model electron reflection and emission as follows.

(i) For each electron hitting an electrode, a pseudo-random number $R_\eta \in [0, 1]$ determines whether the electron is reflected ($R_\eta \leq \eta$) or absorbed ($R_\eta > \eta$). In the case of reflection the radial velocity of the electron is reversed.

(ii) The kinetic energy of the emitted electrons is assumed to be equally distributed in the range 0–$(\mathcal{E}_{ion} - 2\mathcal{W})$. The angle between the direction of emission and the surface normal is denoted by ψ. The projection of the direction of emission onto the electrode surface, that is, the ϑ–z surface, includes an angle of χ with the cylinder axis. Both angles can be expressed using the velocity components v_r, v_ϑ and v_z:

$$\psi = \arctan\left(\frac{(v_\vartheta^2 + v_z^2)^{1/2}}{v_r}\right) \qquad \chi = \arctan\left(\frac{v_\vartheta}{v_z}\right). \quad (3)$$

Emission normal to the surface is favoured above that in other directions; this results in a $\cos\psi$ dependence of the emission current density j_{em}:

$$\mathrm{d}^2 j_{em}(\psi) \propto \cos\psi\, \mathrm{d}^2\Omega \propto \cos\psi \sin\psi\, \mathrm{d}\psi\, \mathrm{d}\chi \quad (4)$$

where $\mathrm{d}^2\Omega$ is a solid angle element. The normalized distribution function of ψ is thus $f(\psi) = 2\sin\psi\cos\psi$. If the influence of the magnetic field on the emission process is neglected, the emission is independent of the emission angle χ, which is therefore equally distributed between 0 and 2π. This model was implemented in the code in the following way. When an ion hits one of the electrodes, it is absorbed. At the inner electrode a secondary electron may be emitted according to the value of a pseudo-random number $R_\gamma \in [0, 1]$ (emission in the case of $R_\gamma \leq \gamma_i$). Four pseudo-random numbers R_E, R_ψ, R_χ, $R_r \in [0, 1]$ are calculated for each emitted electron to determine

$$\psi = \arcsin(\sqrt{R_\psi}). \quad (5)$$

$$\chi = 2\pi R_\chi \quad (6)$$

$$v = \left(\frac{2R_E(\mathcal{E}_{ion} - 2\mathcal{W})}{m_e}\right)^{1/2}. \quad (7)$$

The velocity and position of the electron are then calculated as

$$v_r = v\cos\psi \quad (8)$$

$$v_\vartheta = v\sin\psi\cos\chi \quad (9)$$

$$v_z = v\sin\psi\sin\chi \quad (10)$$

$$r = r_0 + R_r \Delta t v_r. \quad (11)$$

Here v is the speed of the electron and r_0 is the radial position of the inner electrode.

3. Results and discussion

Several discharge simulations were performed for different values of η and γ_i; for brevity, a simulation will be denoted by the pair (η, γ_i). The results are discussed in this section.

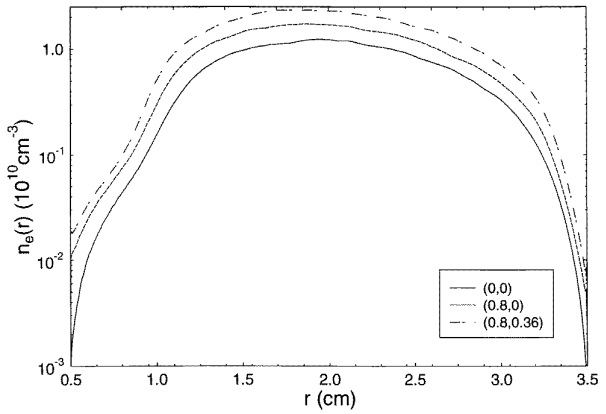

Figure 5. Radial dependence of the electron density n_e for three different discharges with $(\eta, \gamma_i) = (0, 0)$, $(0.8, 0)$ and $(0.8, 0.36)$.

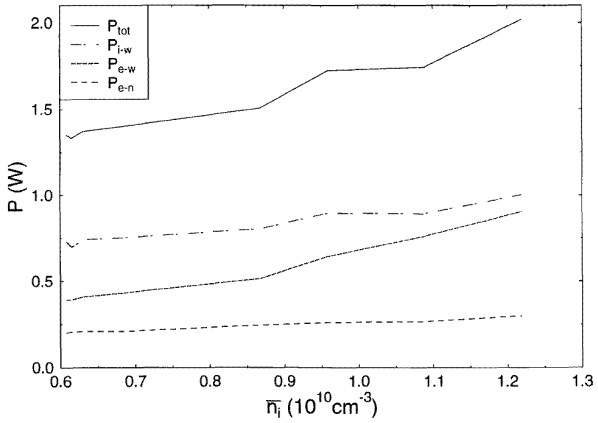

Figure 6. The total power loss P_{tot} in the discharge and the contribution of ion–wall collisions P_{i-w}, electron–wall collisions P_{e-w} and electron–neutral species collisions P_{e-n}.

3.1. Density and power balance

The different parameter sets of the simulations are illustrated in figure 3. Here η and γ_i are plotted against the average ion density $\overline{n_i}$ in the discharge. The ion density increases monotonically with η and γ_i. Therefore $\overline{n_i}$ can be used as a parameter to classify the discharges.

The influence of the electrode processes on the average density in the discharge can be compared by calculating the total production rate S_e of electrons. There are three production processes incorporated in our model:

(i) ionization through electron impact on neutral atoms;

(ii) electron reflection; this can be regarded as electron absorption and subsequent emission of an electron with coordinates dependent on the coordinates of the absorbed electron; and

(iii) secondary electron emission due to ion impact at the inner electrode.

Electrons are created pairwise with the ions in the volume of the discharge, that is, the production rates for electrons and ions are equal:

$$S_{e,ion} = S_i. \tag{12}$$

This is the only production process for ions. In our one-dimensional discharge model, ions are lost exclusively through recombination at the electrodes. If $I_{i,0}$ denotes the ion current to the inner electrode, the probability of one ion emitting a secondary electron is $\gamma_i I_{0,i}/S_i$. This gives an electron production rate of

$$S_{e,\gamma} = \gamma_i I_{0,i}. \tag{13}$$

The total production rate is

$$S_e = S_{e,ion} + S_{e,\gamma} + S_{e,\eta} \tag{14}$$

where the rate of reflected ions $S_{e,\eta}$ depends on S_e:

$$S_{e,\eta} = \eta S_e. \tag{15}$$

Solving equation (14) for S_e yields

$$S_e = S_i \frac{1 + \gamma_i I_{0,i}/S_i}{1 - \eta}. \tag{16}$$

In figure 4, the quotient $Q = S_e/S_i$ is plotted versus $\overline{n_i}$. Q reaches a very high value of up to six, whereas the density varies only by a factor of two. This shows that the influence on the plasma density of (i) electron reflection and (ii) secondary electron emission due to ion bombardment is only moderate. Nevertheless, the density increases monotonically with Q. Looking at the slope of $Q(\overline{n_i})$, the two processes can be distinguished: $\partial Q/\partial \overline{n_i}|_{(i)}$ exceeds $\partial Q/\partial \overline{n_i}|_{(ii)}$ by a factor of four. This shows that in case (i) more electrons are necessary to raise the average ion density in the discharge than in case (ii). The different time behaviour of the two processes is responsible for this: a major characteristic of RF discharges is the strong time-modulation of the electron current at the electrodes. Electrons from the plasma may reach the electrodes only when the electrode potential is close to its positive maximum. The sheath electric field during this part of the RF cycle is small and hence the energy gain of the reflected electrons is small as well. As opposed to the electron current, the ion current is only slightly time-modulated; there is a constant ion current towards the electrodes. This ion current induces a current of secondary electrons which is constant throughout the RF cycle. In this way, electrons are emitted even in the cathodic part of the RF cycle. The strong sheath electric field at this time accelerates the electrons to high energy. Thus the average energy gain per secondary electron exceeds that of a reflected electron in the absence of secondary electron emission. This additional energy causes additional ionization in the discharge and thereby raises the density in the plasma.

Note that secondary electron emission is inefficient when there is no electron reflection at the electrode (see figure 3). The magnetic field causes the emitted electrons to move on a cycloidal trajectory. On this trajectory most of the electrons hit the electrode and are absorbed if no reflection is possible. In this way γ_i is reduced to an effective $\gamma_{i,eff}$ which is to a first approximation proportional to $\eta\gamma_i$.

The radial dependence of the electron density is shown in a logarithmic plot in figure 5 for three discharges with

$(\eta, \gamma_i) = (0, 0)$, $(0.8, 0)$ and $(0.8, 0.36)$. There is no dramatic change in the overall characteristics of the profiles when electron reflection and secondary electron emission are included. The location of each discharge can be distinguished between the quasi-neutral plasma bulk in the centre of the discharge, and the inner and outer sheath, which separate the plasma bulk from the electrodes. The density in the plasma bulk is raised by a factor of two, if electron reflection and secondary electron emission are included. At the same time, the inner and outer sheaths contract slightly. As a consequence, the density gradients at the plasma–sheath boundaries become steeper. The electron density in the sheaths and in the vicinity of the electrodes increases by up to an order of magnitude if electron reflection and secondary electron emission are taken into account.

The increase in density is coupled to an increase in dissipated power, since ions are created in inelastic electron–neutral species collisions. In figure 6 the total dissipated power P_{tot} is shown together with its main components: ion–wall collisions P_{i-w}, electron–wall collisions P_{e-w} and inelastic electron–neutral species collisions P_{e-n}. The major part of the energy is lost through wall collisions of ions which were accelerated in the sheaths. With increasing density the power loss through electron–wall collisions becomes more and more important. This is due to the increasing number of electrons produced in the sheaths and at the electrodes.

The slope $\partial P_{e-w}/\partial \overline{n_i}$ is increased by a factor of 2.5 if secondary electron emission is allowed for. The secondary electrons are accelerated in the sheath electric field. Most of them do not collide with a neutral atom. Therefore they must stay on a cycloidal trajectory which leads them back to the electrode. In this way the average energy per electron deposited at the electrode increases when secondary electron emission is included. The increase of P_{i-w} is due to an increase in the ion current to the electrodes. Inelastic electron–neutral species collisions amount only to about 15% of the total power dissipation.

3.2. Electron energy

The average kinetic energy $\overline{E}$ of the electrons in the discharge is shown in figure 7. The kinetic energy in the bulk plasma is lower than in the sheaths. If electron reflection and secondary electron emission are included, $\overline{E}$ decreases. This decrease is especially pronounced at the plasma–sheath boundary, where the relative drop in kinetic energy is 24% compared to 9% in the centre of the discharge and between 0 and 12% in the sheaths. This is an indication for the beginning of the transition from an α-type to a γ-type discharge. The kinetic energy is distributed from the plasma–sheath boundary to the electrodes and the plasma bulk. In this way the dominant energy gain process changes from electron interaction with the oscillating plasma–sheath boundary [32] to electron acceleration in the sheath field.

Although this transition develops slowly and is not as pronounced as in the case of non-magnetic discharges, it has a notable effect on the energy distribution function

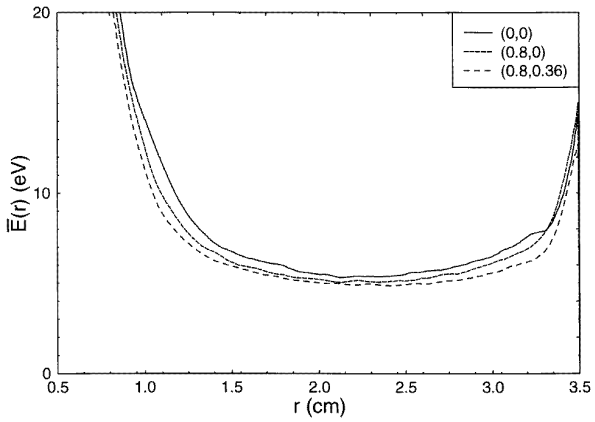

Figure 7. The average kinetic energy $\overline{E}$ of the electrons in the discharge.

of the electrons (EEDF) in the plasma bulk. In figure 8 we look at the Maxwellian character of the EEDF for $(\eta, \gamma_i) = (0, 0)$ in case (a) and $(0.8, 0.36)$ in case (b). Let us denote the EEDF calculated in the simulation by $f(r, E)$. A Maxwellian distribution function with a temperature corresponding to the average kinetic energy at the pertinent position, $\frac{3}{2}kT_e = \overline{E}$, is denoted by $f_{LTE}(r, E)$. Since

$$f_{LTE}(r, E) \propto \sqrt{E} \exp[-E/kT_e(r)] \tag{17}$$

a logarithmic plot of $f_{LTE}(r, E)E^{-1/2}$ is manifested as a family of straight lines with position-dependent slope. Hence any deviation from a straight-line behaviour of $\log[f(r, E)E^{-1/2}]$ is an indication of non-Maxwellian behaviour. To visualize the deviation, figures 8(a) and (b) show

$$\delta(r, E) = \frac{\log[f(r, E)] - \log[f_{LTE}(r, E)]}{\log[f_{LTE}(r, E)E^{-1/2}]} \tag{18}$$

for the two different discharges. $\delta(r, E)$ is positive (light), where $f(r, E)$ contains more electrons than the Maxwellian distribution would predict. It is negative (dark), where $f(r, E)$ fails to reach the number of electrons that a local thermal equilibrium would require. In figure 8(a), $(\eta, \gamma_i) = (0, 0)$, the discharge can be divided into four regions [34]: the inner sheath, the heated bulk, the thermal bulk and the outer sheath. The EEDF in the sheaths is far away from thermal equilibrium because it shows enrichment and depletion of the EEDF throughout the whole energy range observed. The region of the bulk plasma next to the inner sheath exhibits an enrichment of the EEDF for energies above 30–40 eV ('heated bulk'). In contrast, the region next to the outer sheath is well thermalized. Especially the latter region can be described by a fluid model [34]. In figure 8(b), $(\eta, \gamma_i) = (0, 0)$, the sheaths contract and the bulk plasma expands towards the electrodes. In the bulk plasma the deviation of the EEDF from Maxwellian behaviour is very strong. This is due to an increasing energy transport from the sheaths to the bulk. The bulk plasma in this case is difficult to describe with a one-temperature EEDF. Instead of this a two-temperature electron model would be required.

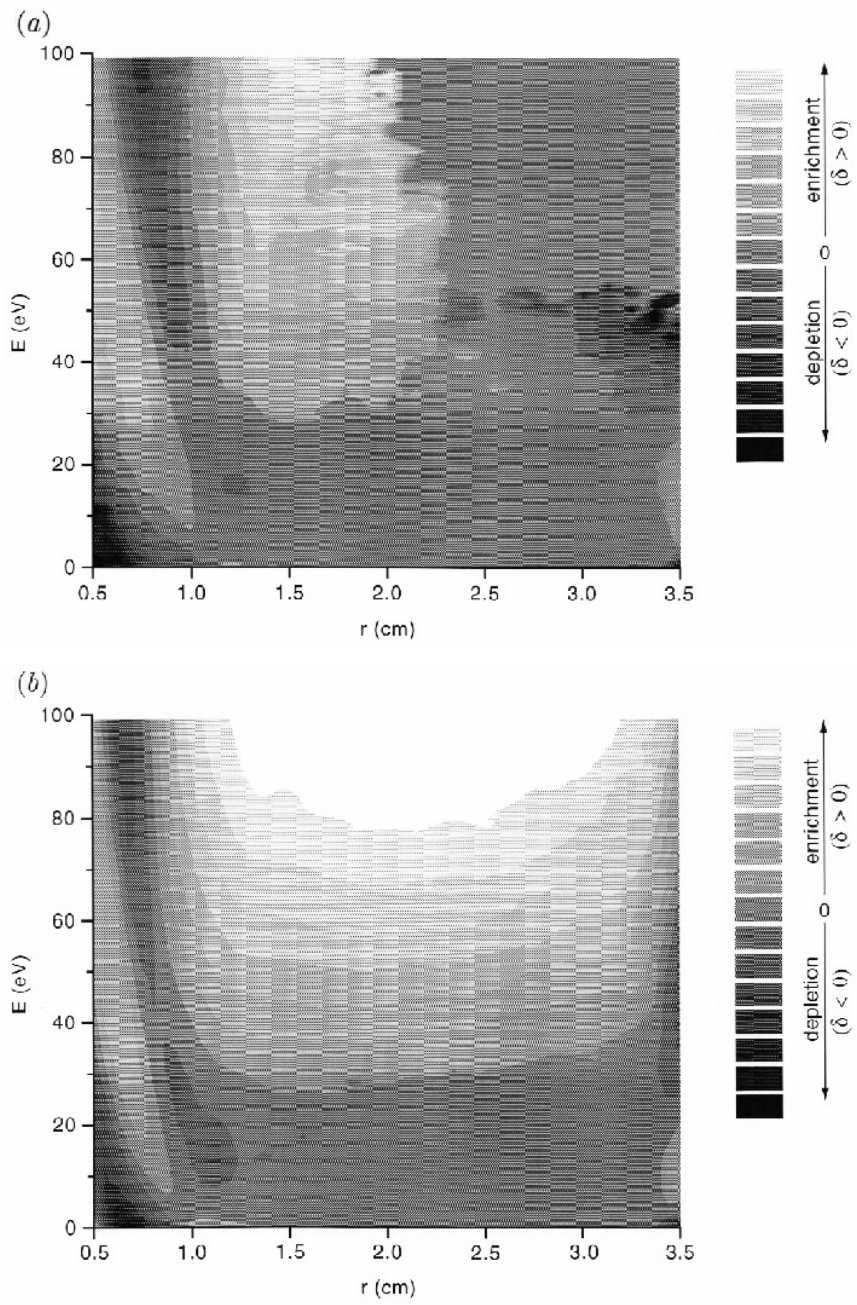

Figure 8. A contour plot of the deviation $\delta(r, E)$ of the distribution function observed in the kinetic simulation from the corresponding Maxwellian distribution function, see equation (18). (*a*) Simulation without electron reflection and secondary electron emission. (*b*) Simulation with $(\eta, \gamma_i) = (0.8, 0.36)$. The δ-scale, given in gray shades, is linearly divided between $\delta = -0.5$ and $\delta = 0.5$.

3.3. Sheath

The electric fields for the three discharges $(\eta, \gamma_i) = (0, 0)$, $(0.8, 0)$ and $(0.8, 0.36)$ are analysed for different phases in the RF period. The electric fields at the phases $\varphi = 0$ and π, see equation (1), are both similar to the cycle-averaged electric field, which we plot in figure 9(*a*). This field is negative and thus prevents the electrons from reaching the electrode. It supports an ion current towards the electrode. The ion current has to be compensated by an equivalent electron current. During the anodic part of the RF cycle ($\varphi = \pi/2$) in figure 9(*b*), the electrons are drawn towards the electrode by a positive electric field. Because of the low electron mobility perpendicular to the magnetic field, only a fraction of the electrons can reach the electrode; just enough to balance the ion current. The gradient of the electric field in the vicinity of the electrode is steeper (and hence the field itself attains a more extreme value) if electron reflection and secondary electron emission are included. This is due to a temporarily negative space charge in the sheath which becomes stronger and approaches the electrode if η and γ_i are increased. In the cathodic part

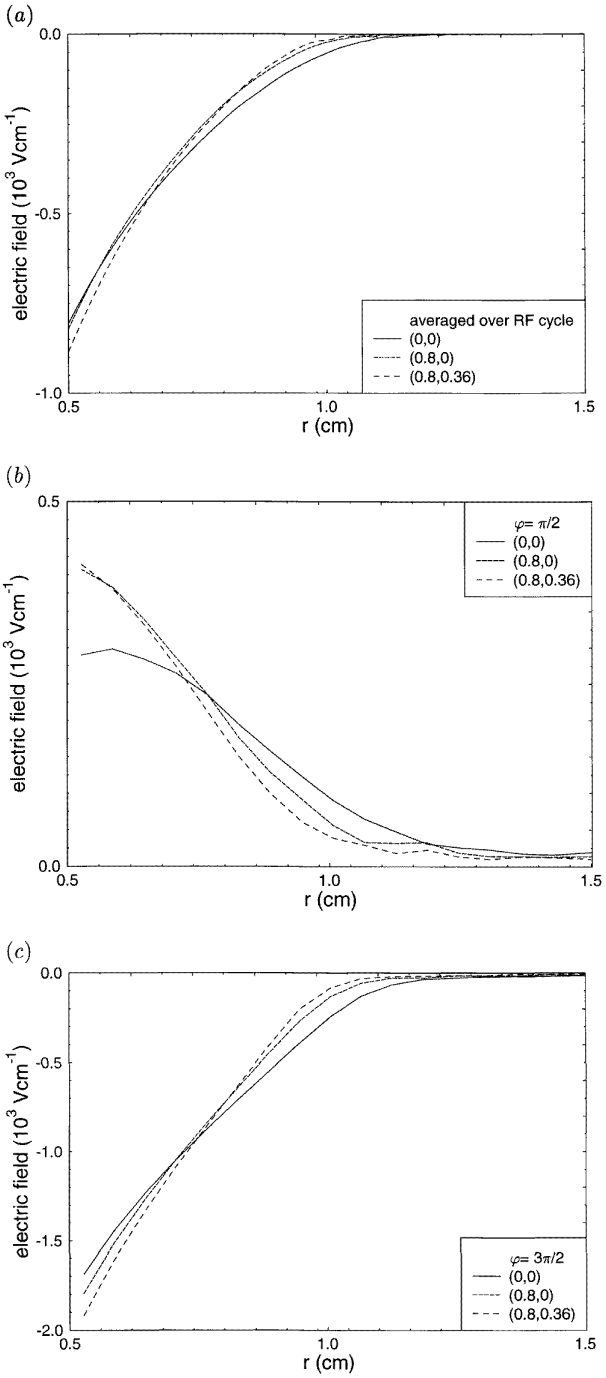

Figure 9. The electric field in the inner sheath region for three discharges (η, γ_i) = (0, 0), (0.8, 0) and (0.8, 0.36): (*a*) averaged over an RF cycle, (*b*) during the anodic part of the RF cycle ($\varphi = \pi/2$) and (*c*) during the cathodic part of the RF cycle ($\varphi = 3\pi/2$).

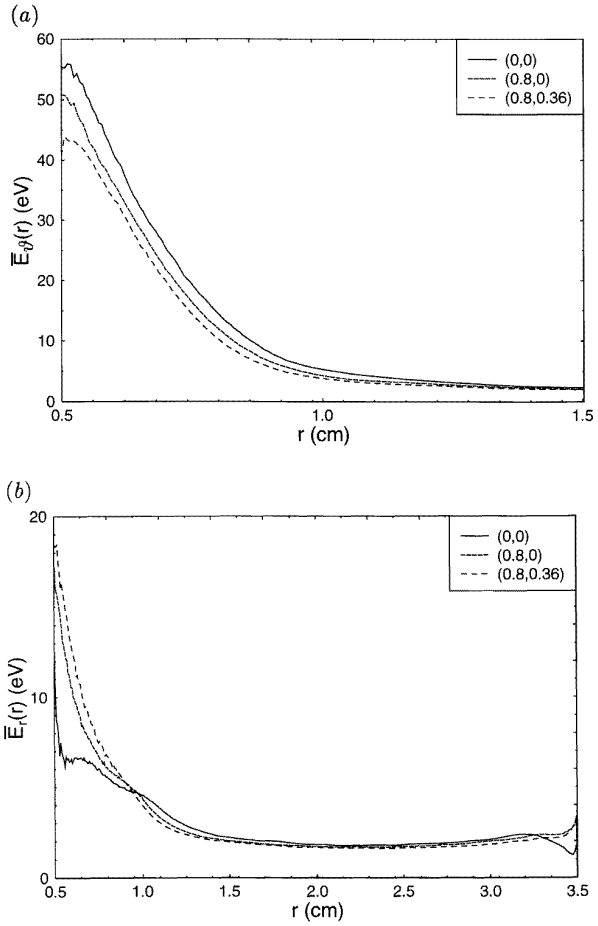

Figure 10. The kinetic energy of the electrons in the inner sheath region averaged over an RF cycle for discharges (η, γ_i) = (0, 0), (0.8, 0) and (0.8, 0.36). The average energy (*a*) in the azimuthal degree of freedom ($\overline{E_\vartheta} = 0.5 m_e v_\vartheta^2$). and (*b*) in the radial degree of freedom ($\overline{E_r} = 0.5 m_e v_r^2$). Note the change of scale in (*b*).

of the cycle ($\varphi = 3\pi/2$) in figure 9(*c*), the electric field reaches an absolute value of 1.9×10^3 V cm^{-1} next to the electrode. Secondary electrons emitted in this part of the RF cycle may gain up to 170 eV in the sheath electric field.

The period averaged kinetic energy of the electrons in the inner sheath was calculated for the same three discharges. The distribution of the energy among the three degrees of freedom: azimuthal $\overline{E_\vartheta} = 0.5 m_e v_\vartheta^2$, radial $\overline{E_r} = 0.5 m_e v_r^2$ and axial $\overline{E_z} = 0.5 m_e v_z^2$ was analysed. Figure 10(*a*) shows the radial dependence of $\overline{E_\vartheta}$ for the three discharges. The energy increases from 2 eV in the plasma to approximately 50 eV at the inner electrode. The high amplitude of the radial RF electric field in the inner sheath together with the axial magnetic field give rise to a time-varying magnetron-drift of the electrons in the azimuthal direction. Due to the low pressure of the discharge the electron–neutral species collision frequency $\nu_{e,n}$ is small compared to ω_{RF}. Therefore the kinetic energy cannot be distributed efficiently among the three degrees of freedom and thermal equilibrium of the electrons cannot be established. In figure 10(*b*) the kinetic energy $\overline{E_r}(r)$ in the inner sheath is plotted. $\overline{E_r}(r)$ increases from the bulk to the inner electrode. Next to the inner electrode, $\overline{E_r}$ is smaller than $\overline{E_\vartheta}$ by a factor of eight in discharge (0, 0). This factor is reduced to about 3.3 in discharge (0.8, 0) and further to about 2.4 in discharge (0.8, 0.36). Due to the reflection of electrons at the electrode, some of the electrons remain in the sheath for a longer period of time. In this

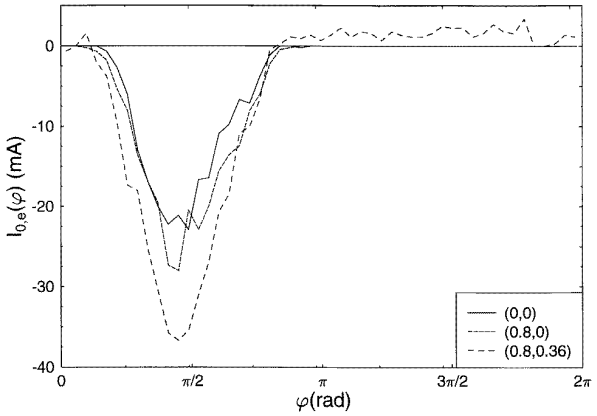

Figure 11. The electron current $I_{0,e}$ at the inner electrode as a function of phase φ in the RF cycle.

way the possibility of an electron–neutral species collision in the sheath increases and the energy distribution among the three degrees of freedom is improved. As a result $\overline{E_\vartheta}$ decreases and $\overline{E_r}$ increases if electron reflection is included. The energy $\overline{E_z}$ has a radial dependence analogous to that of $\overline{E_r}$.

3.4. The inner electrode

In the discharge volume ions and electrons are generated pairwise in electron–neutral species ionizing collisions. The only loss process for these particles is recombination at the electrodes. Therefore the particle currents to the electrodes averaged over an RF cycle have to be equal. The RF mobility of the ions is very low; they move according to the cycle-averaged electric field and the cycle-averaged density and temperature gradients [34]. The electron motion in the sheaths is determined by the temporal behaviour of the electric field. The resulting electron current to the inner electrode is shown in figure 11. It is negative at a phase φ around $\pi/2$; this is the phase of a positive electrode potential, see equation (1). The width of the electron current peak and its amplitude is increased if electron reflection and secondary electron emission are included. When the electrode potential becomes negative and thus prevents the electrons from reaching the electrode, the electron current is reduced to zero. In the case of secondary electron emission, the time-invariable ion current induces a positive electron current which is superposed onto the time-dependent electron current. This leads to a positive electron current outside the anodic part of the RF cycle in the case of secondary electron emission.

We also analysed the backscattered electrons at the inner electrode for the discharges $(\eta, \gamma_i) = (0.8, 0)$ and $(0.8, 0.36)$. Figure 12(a) shows the energy distribution function $f_0(E)$ of the reflected electrons. Additionally the energy distribution function of the ion-induced secondary electrons is plotted (shaded). For the discharge with $(0.8, 0)$ the maximum of the electron energy distribution is obtained for $E = 80$–90 eV and has a half-width of 100 eV. If secondary electron emission is included, the main maximum of the energy distribution of reflected

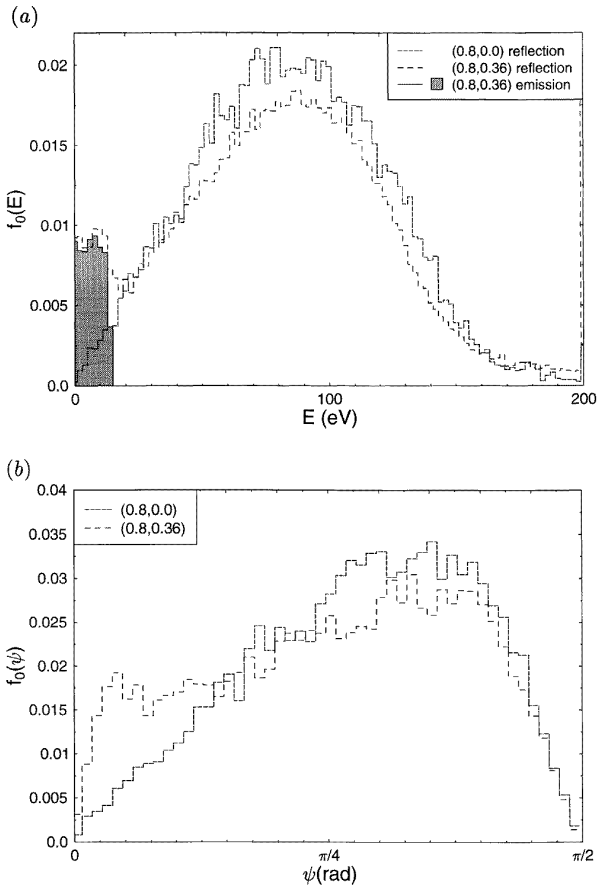

Figure 12. Analysis of backscattered electrons at the inner electrode for discharges $(\eta, \gamma_i) = (0.8, 0)$ and $(0.8, 0.36)$. (a) The energy distribution function $f_0(E)$ of reflected electrons. Additionally the energy distribution function of the ion-induced secondary electrons is shown (grey area). (b) The distribution function of the emission angle $f_0(\psi)$.

electrons remains at the same energy but is less pronounced. An additional maximum is established at low energies $E <$ 20 eV. A comparison with the energy distribution of the emitted secondary electrons shows that these electrons are responsible for the low-energy maximum of the reflected electrons in the discharge $(0.8, 0.36)$. The energy of the emitted secondary electrons for $\gamma_i = 0.36$ is in the range 0–14.76 eV, see equation (2). These low-energy secondary electrons move back to the electrode on cycloidal trajectories. During the short-lasting flight the electrons gain but little energy in the sheath field and thus the energy of the incoming electrons is close to the emission energy. Of the electrons, 80% are reflected elastically and these electrons appear as the low-energy maximum in the total energy distribution function of all reflected electrons.

The distribution function $f_0(\psi)$ of the emission angle ψ of reflected electrons is shown in figure 12(b). The maximum is reached at $\psi_{max} = 63°$, that is, most of the electrons hit the electrode with an oblique angle. This is due to the gyro-motion of the electrons which leads electrons mainly in an azimuthal direction. The angle calculated using the average electron energies at the electrode, $\overline{E_\vartheta} =$ 50 eV, and $\overline{E_z} = \overline{E_r} = 17$ eV in equation (3), corresponds

to the most probable emission angle ψ_{max}. In the case of secondary electron emission an additional maximum occurs at small angles, $\psi = 9^\circ$. The secondary electrons are emitted with a $\cos\psi$ distribution; their cycloidal trajectories intersect the electrode in a direction which is close to the surface normal. Due to the specular reflection of the electrons, their reflection angle ψ is close to 0°.

4. Conclusion and outlook

In the present study we investigated the influence of electron reflection from the electrodes and of ion-induced secondary electron emission on the characteristics of a low-pressure cylindrical RF discharge in a strong magnetic field. It might have been surmised that the effects are small or even absent, since a small electron mobility perpendicular to the magnetic field lines prevents electrons from escaping from the vicinity of the electrodes and influencing the plasma. In fact, the effects found are moderate and do not change the qualitative nature of the discharge. However, quantitative effects are found; thus for instance, the average plasma density could be increased by a factor of two if 80% of electrons incident on the electrodes could be reflected and each ion would emit on the average 0.36 electrons. These material data are large, but not unrealistic. In the experiment, using a discharge of the type described in this paper, an enhancement of the plasma density by a factor of two was found with a suitable choice of the electrode material [16, 35]. This effect was attributed to the high secondary electron emission coefficient of the material chosen.

We could show that the effect of electron reflection from the electrodes is at least as important as ion-induced secondary electron emission for the establishment of a high plasma density. This is due to the low mobility of electrons perpendicular to the magnetic field in a low density plasma. Electrons which are emitted from the electrodes perform a cycloidal trajectory in the crossed electric and magnetic field in the vicinity of the electrodes, in which there is only a slight chance of their performing a collision and escaping into the bulk plasma. A suitably high electron reflection coefficient considerably increases the lifetime of electrons close to the electrodes and hence their chance to escape into the bulk plasma, where they can contribute to ionization and increase the plasma density.

The effect of electron emission in an unmagnetized RF discharge has been studied with great care in the literature. In particular, this effect has been discussed in terms of the transition of an α-discharge towards a γ-discharge; whereas in the latter discharge, secondary electrons escape from the electrodes into the bulk plasma and dominate ionization processes there, ionization in an α-discharge occurs in the sheath edges, where electrons gain energy due to so-called wave-riding or electron sheath collision mechanisms. An analysis of the magnetized plasma considered in the present investigation shows that, due to the low electron mobility perpendicular to the field lines, no true γ-discharge is formed; however, ionization becomes more important in the bulk of the discharge and more high-energy electrons are observed there with increasing electrode emission processes. Although these features are visible, one cannot speak of a true transition from one kind of a discharge to another; the change is rather more gradual.

In summary, we think that the present study has shown that, in strongly magnetized RF discharges with electron reflecting electrodes, the effects of secondary electron emission on the discharge characteristics are qualitatively similar to those in an unmagnetized discharge; quantitatively, they are considerably smaller due to the small electron mobility.

Acknowledgment

We would like to thank the Kernforschungszentrum Jülich, Germany, for assistance in the use of an Intel PARAGON parallel computer.

References

[1] Levitskii S M 1958 *Sov. Phys.–Tech. Phys.* **2** 887
[2] Godyak V A and Khanneh A A 1986 *IEEE Trans. Plasma Sci.* **14** 112
[3] Boeuf J P and Belenguer P 1990 *Nonequilibrium Processes in Partially Ionized Gases* ed M Capitelli and J N Bardsley (New York: Plenum) p 155
[4] Raizer Y P 1991 *Gas Discharge Physics* (Berlin: Springer)
[5] Raizer Y P and Schneider M N 1994 *J. Phys. D: Appl. Phys.* **27** 1457.
[6] Okazaki K, Makabe T and Yamaguchi Y 1989 *Appl. Phys. Lett.* **54** 1742
[7] Belenguer P and Boeuf J P 1990 *Phys. Rev.* A **41** 4447
[8] Young F and Wu C H 1993 *J. Phys. D: Appl. Phys.* **26** 782
[9] Carman R J 1992 *J. Phys. D: Appl. Phys.* **25** 198
[10] Makabe T, Nakano N and Yamaguchi Y 1992 *Phys. Rev.* A **45** 2520
[11] Lukyanova A V, Rakhimov A T and Suetin N V 1991 *IEEE Trans. Plasma Sci.* **19** 197
[12] Surenda M, Graves D B and Morey I J 1990 *Appl. Phys. Lett.* **56** 1022
[13] Sommerer T J, Hitchon W N H, Harvey R E P and Lawler J E 1991 *Phys. Rev.* A **43** 4452
[14] Misium G R, Lichtenberg A J and Lieberman M A 1989 *J. Vac. Sci. Technol.* A **7** 1007
[15] Tochikubo F *et al* 1990 *J. Phys. D: Appl. Phys.* **23** 1184
[16] Korzec D, Engemann J and Rapp J 1992 *Rev. Sci. Instrum.* **63** 3068
[17] Krimke R, Urbassek H M, Korzec D and Engemann J 1994 *J. Phys. D: Appl. Phys.* **27** 1653
[18] Dasgupta A and Bhatia A K 1985 *Phys. Rev.* A **32** 3335
[19] Wetzel R C, Baiocchi F A, Hayes T R and Freund R S 1987 *Phys. Rev.* A **35** 559
[20] Bretagne J, Callede M L G and Puech V 1986 *J. Phys. D: Appl. Phys.* **19** 761
[21] Cramer W H 1959 *J. Chem. Phys.* **30** 641
[22] Hofer W O 1987 *J. Vac. Sci. Technol.* A **5** 2213
[23] Chapman B 1980 *Glow Discharge Processes* (New York: Wiley)
[24] Schou J 1988 *Scanning Microsc.* **2** 607
[25] Devooght J *et al* (eds) 1991 *Particle Induced Electron Emission* vol 1 (Berlin: Springer)
[26] Niedrig H 1982 *J. Appl. Phys.* **53** R15
[27] Oechsner H 1978 *Phys. Rev.* B **17** 1052
[28] Baragiola R A 1993 *Nucl. Instrum. Methods* B **78** 223
[29] Baragiola R A, Alonso E V, Ferron J and Oliva-Florio A 1979 *Surf. Sci.* **90** 240

[30] Birdsall C K and Langdon A B 1985 *Plasma Physics via Computer Simulation* (New York: McGraw-Hill)
[31] Verboncoeur J P, Vahedi V and Alves M P 1995 Technical Report 2, Software Distribution Office, ILP, EECS Department, University of California, Berkeley
[32] Krimke R and Urbassek H M 1995 *IEEE Trans. Plasma Sci.* **23** 103
[33] Brackbill J U and Cohen B I 1985 *Orbit Averaging and Subcycling in Particle Simulation of Plasmas* (New York: Academic)
[34] Krimke R and Urbassek H M 1995 *Plasma Sources Sci. Technol.* to be published
[35] Korzec D 1993 *Fortschrittsberichte VDI* series 9, number 160 (Düsseldorf: VDI) (in German)